

NONTHERMAL X-RAY EMISSION FROM THE SHELL-TYPE SNR G347.3–0.5

PATRICK SLANE¹, BRYAN M. GAENSLER^{2,3,4}, T. M. DAME¹, JOHN P. HUGHES⁵, PAUL P. PLUCINSKY¹, AND ANNE GREEN³*For Publication in The Astrophysical Journal: Accepted 29 April 1999*

ABSTRACT

Recent ASCA observations of G347.3–0.5, an SNR discovered in the ROSAT All-Sky Survey, reveal nonthermal emission from a region along the northwestern shell (Koyama *et al.* 1997). Here we report on new pointed ASCA observations of G347.3–0.5 which confirm this result for all the bright shell regions and also reveal similar emission, although with slightly different spectral properties, from the remainder of the SNR. Curiously, no thermal X-ray emission is detected anywhere in the remnant. We derive limits on the amount of thermal emitting material present in G347.3–0.5 and present new radio continuum, CO and infrared results which indicate that the remnant is distant and of moderate age. We show that our observations are broadly consistent with a scenario that has most of the supernova remnant shock wave still within the stellar wind bubble of its progenitor star, while part of it appears to be interacting with denser material. A point source at the center of the remnant has spectral properties similar to those expected for a neutron star and may represent the compact relic of the supernova progenitor.

Subject headings: ISM: individual (G347.3–0.5) — supernova remnants — X-rays: interstellar

1. INTRODUCTION

While standard wisdom has long held that some significant component of the cosmic ray spectrum is the result of particle acceleration by shocks in SNRs, only recently has compelling evidence of such a process been observed. Studies carried out with the *Advanced Satellite for Cosmology and Astrophysics* (ASCA) have clearly established the nonthermal nature of the emission from the limb-brightened regions of the remnant of SN 1006 (Koyama *et al.* 1995). Both the spectrum and the morphology of the observed X-rays can be explained by models in which synchrotron radiation is produced from electrons with energies up to 100 TeV accelerated by the remnant blast wave (Reynolds 1996), a scenario which is bolstered by the apparent detection of TeV γ -rays from SN 1006 (Tanimori *et al.* 1998).

X-ray spectral results similar to those for SN 1006 are observed for the remnant G347.3–0.5 (Figure 1), a bright SNR discovered in the ROSAT All-Sky Survey (RASS; Pfeffermann & Aschenbach 1996 – the ROSAT catalog source name for the remnant is RX J1713.7–3946). Koyama *et al.* (1997) serendipitously observed the northwest shell of the remnant in a portion of a Galactic Plane survey being conducted with ASCA and found that the emission from this region appears nonthermal; the spectrum is featureless, extends to high energies, and is well described by a power law.

Here we present our new X-ray and radio observations of G347.3–0.5 that cover the entire SNR. In §2 below, we describe the several data sets we have for the remnant. In §3 we discuss the remnant’s distance implied by our CO data and the spectral results from the X-ray observations. Section 4 contains a discussion of the overall picture the data suggest for G347.3–0.5, and the conclusions are summarized in §5.

2. OBSERVATIONS

Nonthermal emission in supernova remnants is usually associated with the presence of a central pulsar-powered synchrotron nebula. SN 1006 appears to present a glaring exception to this scenario, but Cas A also possesses a hard power-law tail (Allen *et al.* 1997), and IC443 harbors a concentration of hard emission (Keohane *et al.* 1997) that appears to be associated with a molecular cloud interaction site. With synchrotron spectra extending to 10 keV and beyond, this implies the presence of electrons with energies as high as 100–200 TeV for typical interstellar magnetic fields. The origin of this emission is of considerable significance both in terms of the long-surmised source of cosmic rays and because it raises questions about what special conditions are responsible for such production in such a limited number of SNRs. Like SN 1006 (but unlike Cas A or IC443), the nonthermal emission from G347.3–0.5 *dominates* the X-ray flux. This SNR thus presents significant evidence for particle acceleration which may lead to a confirmation of the long-suspected connection with the origin of cosmic rays. However, in contrast to SN 1006, whose age, distance, and progenitor type are known, G347.3–0.5 is an unfamiliar beast. To understand how and why (or even if) it is acting as a cosmic ray accelerator, we need to establish the basic fundamentals of its character.

2.1. X-Ray

G347.3–0.5 was first discovered in the RASS data (Pfeffermann & Aschenbach 1996). A follow-up 3 ks pointed observation was then carried out with the Position Sensitive Proportional Counter (PSPC), providing a good map of the ~ 60 arcmin diameter remnant (Figure 1). The spectral results were inconclusive, however, being unable to distinguish between a thermal or nonthermal origin for the soft X-ray emission. The

¹Harvard-Smithsonian Center for Astrophysics, 60 Garden Street, Cambridge, MA 02138²Center for Space Research, Massachusetts Institute of Technology, Cambridge, MA 02139³Astrophysics Department, School of Physics A29, University of Sydney, NSW 2006, Australia⁴Australia Telescope National Facility, CSIRO, PO Box 76, Epping, NSW 1710, Australia⁵Department of Physics and Astronomy, Rutgers, The State University of New Jersey, 136 Frelinghuysen Road, Piscataway, NJ 08854-8019

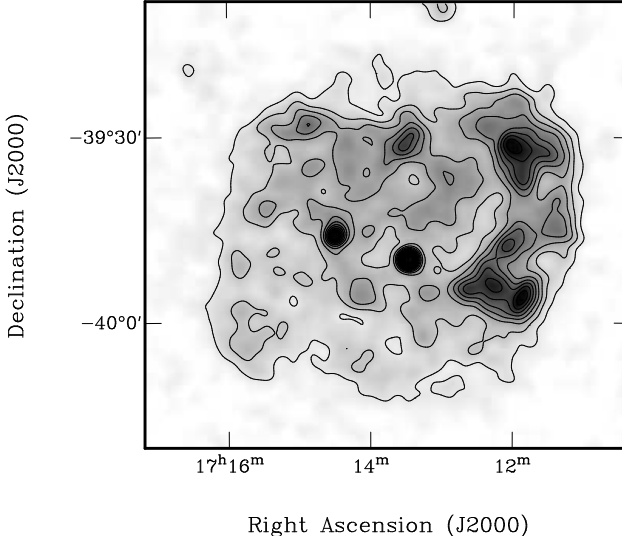


FIG. 1.— ROSAT PSPC image of G347.3–0.5. Two point-like sources are seen in the central regions. The eastern-most source is associated with a star while the central source is unidentified. ASCA observations reveal strong nonthermal emission from the two bright regions along the western limb as well as weak nonthermal emission from the rest of the interior. Contour levels start at 1.44 counts $\text{arcmin}^{-2} \text{ s}^{-1}$ and increase inward in steps of 1.15 counts $\text{arcmin}^{-2} \text{ s}^{-1}$.

PSPC also reveals two point-like sources in the field of the remnant. The first, 1WG AJ1714.4–3945, has a very soft spectrum and appears to be associated with a star (Pfeffermann & Aschenbach 1996). We will not discuss it further. The second source, 1WG AJ1713.4–3949, which is located near the center of the remnant at position 17^h 13^m 28^s, $-39^\circ 49' 46''$ (epoch J2000 here and henceforth), has no reported counterpart. The brightest cataloged object near the X-ray source is ~ 10 arcsec away and has an optical magnitude $m_B = 21.5$ ($m_R = 18.4$). This separation is consistent with the expected position errors for the PSPC source given the point spread function of the detector as well as aspect reconstruction errors. The large X-ray to optical flux ratio is consistent with what might be expected for a neutron star. A stellar counterpart is virtually ruled out for such a ratio (Stocke et al. 1991), but a background extragalactic source remains a possibility.

We observed G347.3–0.5 with ASCA on 1997 March 25 for a total of 50 ks using three pointings of 10 ks duration and one (in the fainter southeast region) of 20 ks duration, which resulted in complete coverage by the Gas-Imaging Spectrometer (GIS). Complimentary chips on the CCDs were used to image the entire Solid-state Imaging Spectrometer (SIS) field of view; nevertheless, complete coverage of the remnant was not possible with the SIS. Risetime information for the GIS was sacrificed in order to provide improved temporal resolution so that timing analysis could be carried out on the central source. After standard screening procedures for the GIS and SIS data, we performed spectral fits for several distinct spatial regions defined as follows: NW - a box surrounding the bright region in the northwest which was first studied by Koyama et al. (1997); SW - a box surrounding the bright region in the southwest; PTSRC - a 3 arcmin radius circle centered on the central source; and EAST - combined data from two circles in the northeast and southeast regions of the remnant. These regions are shown schematically

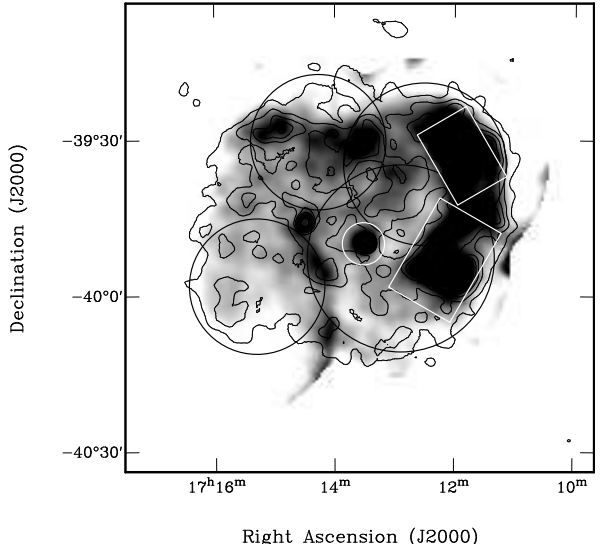


FIG. 2.— ASCA GIS image of G347.3–0.5 with PSPC contours. Regions used for spectral studies are indicated. Boxes along the western limb were used for the NW and SW regions (see text). Two circles from the eastern half of the remnant were used for the EAST region and a circle around the central point source was used for the PTSRC region. For deriving upper limits to the thermal emission for the entire SNR, the four black circles were used with the white circle excluded.

in Figure 2 where we present the GIS image. (Also shown are additional circles used in combination with EAST to establish limits on the total thermal emission; see §3.2.2.) The corresponding spectra are shown in Figure 3.

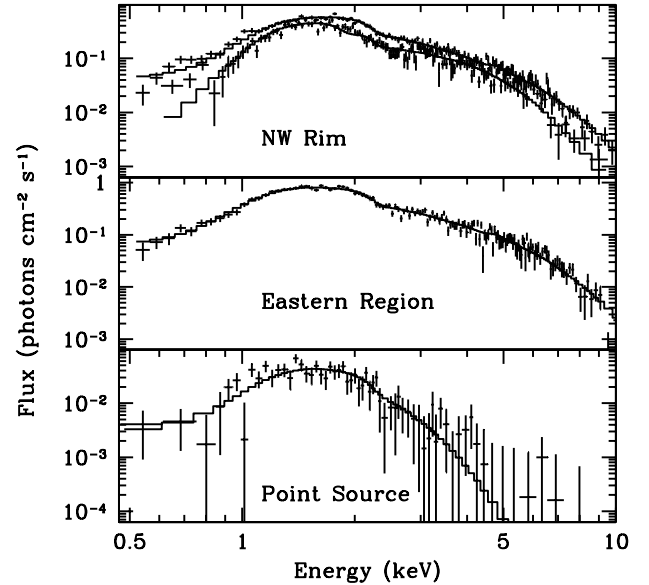


FIG. 3.— ASCA spectra from distinct regions of G347.3–0.5 (see Figure 2) along with best-fit models. Top Panel: GIS (upper) and SIS (lower) from NW shell. Spectrum is well described by a power law (shown as histogram) and is indistinguishable from spectrum of SW shell (not shown). Middle Panel: GIS spectrum from eastern region of remnant along with best-fit power law model. Lower Panel: GIS spectrum of central point-like source along with best-fit blackbody model.

TABLE 1
G347.3–0.5 SPECTRAL PARAMETERS

Region	$N_H (\times 10^{21} \text{ cm}^{-2})$	Γ (photon)	$F_x(0.5\text{--}10 \text{ keV})$
NW Rim	8.1 ± 0.4	$2.41^{+0.05}_{-0.04}$	$1.6 \times 10^{-10} \text{ erg cm}^{-2} \text{ s}^{-1}$
SW Rim	7.9 ± 0.5	2.40 ± 0.05	$2 \times 10^{-10} \text{ erg cm}^{-2} \text{ s}^{-1}$
Eastern Region	5.6 ± 0.4	2.17 ± 0.05	$3 \times 10^{-10} \text{ erg cm}^{-2} \text{ s}^{-1}$

Unlike the line-dominated X-ray spectra typical of SNRs, the spectra for G347.3–0.5 are clearly featureless and extend to at least 10 keV, where the ASCA effective area becomes very small. For each region, we performed joint fits to data from each GIS detector as well as to the associated PSPC data from the same spatial region of the remnant. A power law spectrum provides an excellent fit to each spectral region of the remnant. The NW and SW regions display virtually identical spectra while that for the eastern region appears to have a flatter spectral index and somewhat lower absorption. The best-fit spectral values are listed in Table 1. Addition of a thermal component (Raymond & Smith 1977) to the spectral model does not result in a significant improvement in the fit; there is no significant evidence for thermal emission from any portion of the SNR. We note that a pure thermal bremsstrahlung model (e.g., an exponential with gaunt factor) yields a considerably larger value of χ^2 than does the power law model (e.g., for the SW region, $\chi^2 = 364$ for 293 degrees of freedom compared with $\chi^2 = 312$ for the power law model).

The SIS data provide higher sensitivity for detection of line features in the spectra due to its better spectral resolution compared to the GIS. However, due to the extended nature of the emission, the number of counts in any particular chip is small. Further, background measurements were possible for only two of the chips and these were used as representative background for analysis of data from other chips. Variations in the spectral characteristics of each chip, plus possible spatial variations in the cosmic and Galactic X-ray background emission, thus introduce larger uncertainties than would be obtained with independently measured backgrounds. We have carried out fits to the SIS data from the NW region, the SW region, and for the northeast region. In each case, the SIS fits show no evidence of spectral lines and the power-law fit parameters are in reasonable agreement with those obtained from the joint GIS/PSPC fits.

The nonthermal nature of the emission from all regions of the remnant is quite peculiar. Unlike SN 1006, where thermal emission is found in the central regions, any such component from G347.3–0.5 is apparently overwhelmed by the nonthermal emission. We discuss this surprising result in §3.

TABLE 2
BLACKBODY MODEL FOR 1WGAJ1713.4–3949

Parameter	Value
N_H	$5.2^{+1.8}_{-1.6} \times 10^{21} \text{ cm}^{-2}$
kT	$0.38 \pm 0.04 \text{ keV}$
$K^{(a)}$	25^{+20}_{-10}
$F_x(0.5\text{--}5.0 \text{ keV})$	$5.3 \times 10^{-12} \text{ erg cm}^{-2} \text{ s}^{-1}$

(a) $K = (R_{\text{km}}/D_{10})^2$ where R is radius of emitting region in km and D_{10} is distance in units of 10 kpc

The spectrum from the unidentified central source 1WGAJ1713.4–3949 is not well constrained by the data. Joint fits to the SIS/GIS/PSPC data yield acceptable fits for power-

law, Raymond-Smith, bremsstrahlung, and blackbody models. The blackbody model yields the lowest overall χ^2 fit (though only marginally lower than the other models), and we summarize these fit parameters in Table 2 for use in discussing a neutron star scenario for this source in §3.2.3. However, we note that additional observations are required to obtain a higher fidelity characterization of the spectral properties.

2.2. IR and Radio

We have also investigated the infrared emission from the region with the Infrared Astronomical Satellite (IRAS) $60\mu\text{m}/100\mu\text{m}$ ratio (Figure 4). An enhancement of this ratio, indicative of hot dust, has been shown to be a powerful discriminator of remnant emission against the background emission of the Galactic plane (Saken, Fesen, & Shull 1992; Slane, Vancura, & Hughes 1996). The infrared emission in the inner Galactic disk is intense and complicated, but as Figure 4 shows, there is a clear enhancement of the $60\mu\text{m}/100\mu\text{m}$ ratio coincident with the remnant. The strongly enhanced ratio to the northwest of the remnant is due to the H II region G347.61+0.20 (Lockman 1979), which may be associated with the same molecular cloud as the remnant (see §3.1).

Radio maps from the Parkes-MIT-NRAO (PMN) 6 cm survey (Condon, Griffith, & Wright 1993) reveal complex emission from the region surrounding the remnant, but we find very good morphological correspondence with the infrared emission, particularly for the regions directly west and northwest of the remnant. To better delineate any radio emission corresponding to the X-ray remnant, we have carried out 843 MHz observations using the Molonglo Observatory Synthesis Telescope (MOST; Robertson 1994). The synthesis was carried out on 1997 May 27, with the telescope in its Wide Field mode of operation (Large et al. 1994). The resulting map (Figure 5) reveals regions of faint emission which extend along most of the SNR perimeter, with the most distinct emission corresponding to the bright X-ray regions in the northwest and southwest. Considerable contributions from sidelobes, baseline errors, and grating rings from surrounding sources result in a rather high noise level of $\sim 4 \text{ mJy beam}^{-1}$; the contrast has been adjusted considerably to show the faint shell emission.

The brightest regions of emission within the confines of the X-ray contours are found along two arcs in the northwest. These are concentrated along the edges of the brightest X-ray emission. Arc 1 is centered at approximately $17^{\text{h}} 12^{\text{m}} 46^{\text{s}}$, $-39^{\circ} 25' 49''$. We estimate a surface brightness range of $\sim 17\text{--}27 \text{ mJy beam}^{-1}$ ($27\text{--}43 \text{ mJy arcmin}^{-2}$) with $\sim 10\%$ uncertainty in these values. Arc 2, centered at $17^{\text{h}} 11^{\text{m}} 27^{\text{s}}$, $-39^{\circ} 32' 36''$ has a surface brightness range $\sim 56\text{--}82 \text{ mJy beam}^{-1}$ ($90\text{--}130 \text{ mJy arcmin}^{-2}$) with similar uncertainty. This arc appears to be most closely correlated with the bright X-ray emission and, although its east-west elongation is curiously askew with respect to the perceived SNR shell at this location, the radio filament does overlay a filament of X-ray emission at this position. An upper limit to any radio counterpart to the unidentified

FIG. 4.— IRAS 60 μm /100 μm ratio image with PSPC contours overlaid. A marginal enhancement in the ratio appears over the interior of the remnant, but significant emission is seen outside the western limb possibly indicating the presence of adjacent cool material.

X-ray point source 1WGA J1713.4–3949 is 15 mJy (5σ). The intense emission beyond the NW limb of the remnant corresponds to the same H II region, G347.61+0.20, that was evident in the IRAS map (Figure 4).

Additional radio observations of G347.3–05 with higher resolution and sensitivity have been carried out with the Australia Telescope Compact Array. Analysis of these data is in progress and will be reported in a future publication.

2.3. CO Line Measurements

To further constrain our picture of the environment surrounding the remnant, we have used observations of the $J = 1 \rightarrow 0$ rotational transition of CO (at 115 GHz), the best large-scale tracer of interstellar molecular gas, from the CfA-Chile 1.2 m telescope (Bronfman et al. 1989). Figure 6 is a map of total molecular column density over a wide section of the inner Galaxy centered on the SNR. It is noteworthy that the SNR coincides very closely with the largest and deepest hole in the molecular column density near the Galactic plane in the inner fourth quadrant. Since the CO emission in the direction of the remnant is complex and extends over $\sim 200 \text{ km s}^{-1}$ in radial velocity, it is difficult to determine which individual molecular cloud or clouds, if any, along the line of sight might be associated. The most likely candidates based on the morphology of the CO and

FIG. 5.— MOST image of radio emission at 843 MHz, with PSPC contours. Emission from the bulk of the SNR rim can be seen with particular enhancements along the west/northwest regions where bright nonthermal X-ray emission is seen. Bright emission outside of the western limb corresponds well with the observed infrared emission from this region.

X-ray emission are a pair of clouds at -94 km s^{-1} and a third at -69 km s^{-1} (Figure 7). Given that giant molecular complexes with active star formation sometimes have total velocity extents of 30 km s^{-1} (e.g., W44; Dame et al. 1986), it is possible that all three of these clouds are part of the same molecular complex that gave birth to the H II region G347.61+0.20 and the SNR, with one or more of the clouds significantly perturbed in velocity. The cloud at -69 km s^{-1} abuts the region of strongest X-ray and radio enhancement, suggesting that the remnant may be expanding into this cloud. It is worth noting that a compact region of anomalous-velocity emission extending to -200 km s^{-1} is seen in both 21 cm (Burton 1985) and CO (Bronfman et al. 1989) emission along the line of sight to the remnant.

FIG. 6.— Total molecular column density over a wide section of the fourth Galactic quadrant around G347.3–0.5. Molecular column density, $N(\text{H}_2)$, was derived from velocity-integrated CO intensity, W_{CO} , using a conversion factor of $N(\text{H}_2)/W_{\text{CO}} = 1.9 \times 10^{20} \text{ cm}^{-2} \text{ K}^{-1} \text{ km}^{-1} \text{ s}$. (Strong & Mattox, 1996). The CO data are from the surveys of Bronfman et al. (1989) and Bitran et al. (1997). The contours are logarithmically spaced at $34, 60, 107, 190, 224, \text{ & } 600 \times 10^{20}$ molecules cm^{-2} . The lowest contour was chosen well above the instrumental noise ($\sim 9\sigma$) to emphasize the relatively low molecular column density toward G347.3–0.5 (plus sign).

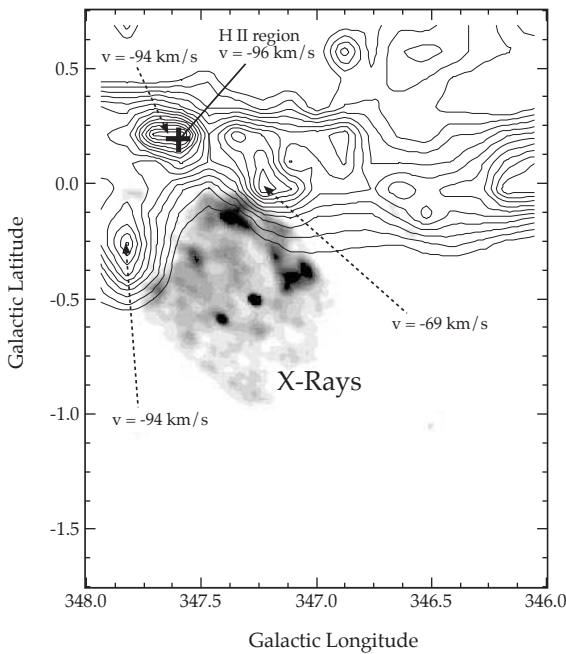


FIG. 7.— Contours of CO intensity integrated over the velocity range -100 to -50 km s^{-1} , from the survey of Bronfman et al. (1989). The contours are spaced every 5 K km s^{-1} , starting at 15 K km s^{-1} . The ROSAT PSPC image is shown in grayscale. The molecular clouds that seem most likely to be associated with G347.3–0.5 are labeled with their LSR velocities. The H II region G347.61+0.20 is marked by a “+” sign.

Given their proximity both in projected position on the sky and in velocity, the pair of clouds at -94 km s^{-1} are almost certainly associated with each other, and with the H II region G347.61+0.20, which has a recombination-line velocity of -96 km s^{-1} (Lockman 1979). An association between the SNR and the pair of clouds at -94 km s^{-1} is suggested by the presence of massive star formation in one of them, as evidenced by the H II region, and by an enhancement of the CO(2–1)/CO(1–0) line ratio in the other. Studies of molecular clouds in the Galaxy find values generally below 1 for the ratio $R = W_{\text{CO}(2-1)}/W_{\text{CO}(1-0)}$. Sakamoto et al. (1995) find a mean value of 0.66 with a variation from 0.5 to 0.8 that has some dependence on Galactocentric distance. Chiar et al. (1994) find a value of 0.85 ± 0.63 from their study of molecular clouds in the Scutum arm of the Galaxy. On the other hand molecular clouds that appear to be undergoing interactions with SNRs (e.g., W44 and IC443; Seta et al. 1998), show an enhanced R ratio (>1.2) that is indicative of shocked material in the molecular gas. We obtained CO(2–1) spectra over the range $l = 346.5$ to 348.5 , $b = -0.5$ to 0.5 , on a 0.25 degree grid (Handa & Hasegawa 1999, private communication) from the University of Tokyo 0.6 m telescope on La Silla, Chile, which has the same angular resolution at the CO(2–1) line as the CfA-Chile 1.2 m at the CO(1–0) line. Over the range for which CO(2–1) spectra were available, the mean R value was determined to be 0.60 ± 0.37 . However, the largest values of R were associated with the cloud at -94 km s^{-1} : in particular, toward $l = 348$, $b = -0.25$, a value of $R \sim 2$ is found near -85 km s^{-1} , in the wing of a strong (4 K) and well-defined CO(1–0) line near -94 km s^{-1} . Such an enhancement in the wing of the CO line is suggestive of

an interaction with the SNR shock wave (Seta et al. 1998). We note that no enhanced R value is observed for the cloud at -69 km s^{-1} which appears along the line of sight to the brightest X-ray limb. However, the CO(2–1) data are coarsely spaced (every 1/4 degree); more sensitive and closely spaced spectra in this region may reveal such an enhancement and are of considerable interest.

3. ANALYSIS

3.1. Distance to G347.3–0.5

Koyama et al. (1997) compare their measurement of the column density toward G347.3–0.5 (which is in good agreement with the values we report here) with the total N_H in the direction of the Galactic center to estimate a distance of 1 kpc to the remnant. We argue that a distance as small as this is unlikely, based on several lines of evidence. Like Koyama et al. (1997) we first consider the distance estimate based on the X-ray derived column density. The total line-of-sight column density in the direction of G347.3–0.5 is $N_H = 1.2 \times 10^{22}$ cm^{-2} based upon H I observations (Dickey & Lockman 1990) and confirmed by CO measurements (Bronfman et al. 1989). This relatively low value is consistent with the presence of a hole in the molecular column density in this direction mentioned earlier (see also Fig 6). The N_H value we measure for G347.3–0.5 ($\sim 8 \times 10^{21}$ cm^{-2} , see Table 1) is a significant fraction of the total column through the Galaxy and so the distance to the remnant must be considerably more than 1 kpc.

We have just argued in the preceding section that the remnant, the H II region, and the complex of three molecular clouds in this direction are all likely to be physically associated. This provides an opportunity to obtain a quantitative estimate for the distance to the remnant. From the rotation curve of the Galaxy (Burton 1988), the pair of clouds at -94 km s^{-1} lie at a distance of $D = 6.3 \pm 0.4$ kpc or $D = 10.4 \pm 0.4$ kpc. Whether the near or far kinematic distance is appropriate can be resolved in favor of the former by noting that molecular absorption measurements place the associated H II region at a distance of 6.3 kpc (Lockman 1979, adjusted to the Burton 1988 rotation curve and $R_0 = 8.5$ kpc). The cloud at -69 km s^{-1} has a near kinematic distance of 5.4 kpc, assuming that its radial velocity is purely due to Galactic rotation. Therefore we adopt a distance of 6 kpc for the distance to G347.3–0.5, with the warning that this is uncertain by at least ± 1 kpc. In the following we present results in terms of $D_6 = D/6$ kpc.

3.2. X-Ray Emission Characteristics

3.2.1. Nonthermal Emission

The nonthermal X-ray emission from G347.3–0.5 strongly indicates that the SNR shock is accelerating particles to very high energies. The electron energy associated with synchrotron photons radiated at energy E_x is

$$E_e \approx \frac{300 \text{ TeV}}{B_{\mu\text{G}}^{1/2}} \left(\frac{E_x}{1 \text{ keV}} \right)^{1/2}.$$

With observed photon energies up to 10 keV, the spectrum for G347.3–0.5 thus indicates the presence of electrons with energies as high as 300 TeV for typical magnetic fields of $\sim 10 \mu\text{G}$. If protons are accelerated to similar energies, it would appear that G347.3–0.5 may be accelerating cosmic rays up to energies near the “knee” in the cosmic ray spectrum at $\sim 10^{15}$ eV. The total energy associated with the X-ray producing electrons

is of order $10^{45} D_6 B_{\mu G}^{-3/2}$ erg which is a small fraction of the mechanical energy released in the supernova explosion.

As noted in Table 1, the spectral index for the emission from the bright regions along the western limb of G347.3–0.5 appears to be steeper than that for the rest of the diffuse emission from the SNR. The column density from the spectral fits also differs between the two regions. When N_H is fixed to the value determined for the NW region, the photon index derived for the eastern region is $\Gamma = 2.4$, the same as that for the regions along the western limb. However, the χ^2 for the fit is considerably higher and the residuals clearly indicate difficulty with such a high absorption value for the eastern region. A variation in column density is not hard to reconcile; many SNRs exhibit such spatial variations in the foreground absorbing column (e.g., Roberts et al. 1993). For G347.3–0.5 this interpretation is particularly reasonable, since the regions indicating higher column density (i.e., the NW and SW enhancement regions) lie closest to the Galactic plane (see Figure 7). Variations in spectral index are also well-understood for synchrotron nebulae where the finite radiating lifetimes of electrons accelerated by a central pulsar result in a steepening of the spectral index with distance from the electron injection point (e.g., Kennel & Coroniti 1984; Slane, Bandiera, & Torii 1998). For synchrotron nebulae the steepening of the spectrum goes along with a decrease in brightness. For G347.3–0.5, however, no obvious injection point is evident, and the steeper index appears to be concentrated along the bright western limb. A synchrotron lifetime argument thus appears problematic in that the brightest synchrotron region (i.e., the western limb) would also have to be “older.” For completeness we note that the nonthermal X-ray emission from SN 1006, with a photon index $\Gamma = 2.95 \pm 0.20$, is steeper than spectra measured here for G347.3–0.5.

3.2.2. Thermal Emission

Although the bright rim regions of SN 1006 are dominated by synchrotron emission, ASCA studies of the interior reveal the line-dominated X-ray thermal component expected from the hot shocked gas characteristic of SNRs (Koyama et al. 1995). Our ASCA observations of G347.3–0.5 reveal no such component. The lack of measurable thermal emission sets limits on the amount of hot material, and thus on the density of the region in which the SNR evolved. This is illustrated in Figure 8 where we have plotted upper limits to the thermal emission measure as a function of temperature based upon our spectral analysis. For the curve plotted as the solid histogram in Figure 8, we have combined data from the GIS detectors using regions that cover most of the remnant (but not the bright regions along the western limb – see Figure 2) and determined 3-sigma upper limits to the amount of thermal emission, assuming normal solar composition, that could be added to the model. The resulting normalization for this thermal component was then scaled by a factor of two to account for the incomplete coverage of the remnant that our spectral extraction regions gave. As indicated in Figure 2, the spectral regions actually cover more than 50% of the area of the SNR, so the upper limits shown are quite conservative.

Under some assumptions about the three-dimensional geometry of the remnant, the upper limit on the emission measure can be converted into a limit on the mean density of the ambient medium. For G347.3–0.5 we assume a spherical shell geometry with a measured angular radius of $\theta_r = 30'$ and an estimated shell thickness equal to $\theta_r/23$. (Note that the factor 23 was chosen for numerical agreement with the integrated emis-

sion measure for a Sedov solution.) For the range of allowed emission measures, we then calculate that the hydrogen number density of the ambient preshock medium in the strong shock limit (i.e., assuming the density jump across the shock front is a factor of 4) is in the range $n_0 = 0.014\text{--}0.28 D_6^{-1/2} \text{ cm}^{-3}$. The lower bound on the ambient density corresponds to temperatures of ~ 0.75 keV, while the upper bound corresponds to the lowest temperature bin in Figure 8.

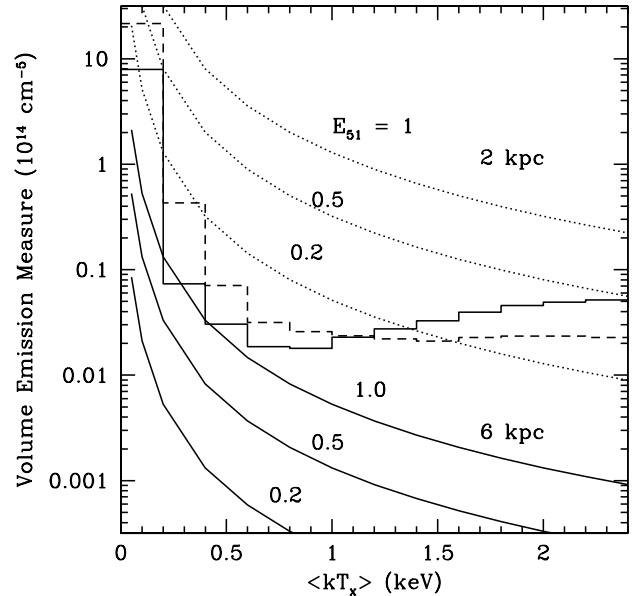


FIG. 8.—Upper limit to derived emission measure plotted as a function of temperature. The two histograms correspond to limits derived for the entire SNR (solid) based upon scaling results which exclude the bright regions (see text), and for the bright northwest region (dashed). Also shown are curves for models derived assuming a Sedov solution. Solid (dotted) curves correspond to a distance of 6 kpc (2 kpc) with E_{51} varying from 0.2 (lower) to 1.0 (upper).

Also plotted in Figure 8 are model curves for explosion energies $E_{51} = 0.2, 0.5$, and 1.0 (in units of 10^{51} erg) assuming a distance of 6 kpc (solid curves) and 2 kpc (dotted curves) under the assumptions that the remnant is in the Sedov (1959) phase of evolution and the electrons and ions share the same temperature behind the shock front. We see that the derived upper limits are not inconsistent with the model curves for our preferred distance of 6 kpc. That is, for the range of parameter space shown, the lack of detectable thermal emission is expected for a Sedov-phase SNR; as with SN 1006, the thermal emission simply pales in comparison to the bright nonthermal emission. For such an interpretation, however, the density of the ambient medium must be very low, as we found above.

The derived upper limits on emission measure appear to rule out a Sedov solution for G347.3–0.5 if the remnant is at a distance of 2 kpc. The only acceptable solution requires an unusually low explosion energy and a rather hot remnant, $kT_x \gtrsim 1.5$ keV. However this conclusion is sensitive to the assumption of temperature equilibration between electrons and ions in the post-shock gas. The alternative scenario, wherein the electrons and ions acquire the same mean thermal velocity behind the shock front and then share energy slowly through Coulomb collisions (see Spitzer 1978), will result in the mean

electron temperature in the remnant (kT_x) lagging considerably behind the post-shock temperature of the ions. In this situation the measured electron temperature does not reflect the actual shock velocity and, in fact, it has been shown (Cox & Anderson 1982) that the electron temperature has an extremely weak dependence on the shock temperature. Furthermore, because the equilibration timescale is inversely proportional to the electron density, the effects of non-equilibration are greatest for low density remnants, which is precisely the situation we have here for G347.3–0.5. Although a detailed analysis of the effects of non-equilibration will be addressed in a future article, we make the following brief comments here. The curves for the Sedov solution shown in figure 8 are substantially modified if equilibration on Coulomb collisional timescales is assumed. First of all, there are no high temperature solutions for reasonable values of the explosion energy ($E_{51} < 2$) anywhere in the range of emission measures plotted. Second, it is not possible to rule out a Sedov solution as a model for the remnant if it is at a distance of 2 kpc. For example, for this distance and a mean temperature of $kT_x = 0.5$ keV, emission measures in the allowed range $0.01\text{--}0.03 \times 10^{14} \text{ cm}^{-5}$ predict ranges for the explosion energy of $E_{51} = 1.4\text{--}2.2$ and the remnant's age of 2100–3400 yrs. Lower values of the mean temperature are also acceptable and result in a broad range of possible dynamical states that, in general, encompass smaller values of the explosion energy and larger values of the age. For a distance of 6 kpc, a reasonable dynamical state for G347.3–0.5 is possible for a mean temperature of $kT_x = 0.3$ keV and emission measures in the allowed range $0.003\text{--}0.07 \times 10^{14} \text{ cm}^{-5}$. Within this range the explosion energy varies in the range $E_{51} = 2.2\text{--}1.7$ and the remnant's age lies between 18,700 yrs and 40,600 yrs. So in conclusion to this discussion, the lack of detected thermal emission from G347.3–0.5 can be reconciled with a broad range of reasonable dynamical evolutionary states, possible remnant ages, and distances as long as the mean ambient density around the remnant is low. This would appear incompatible with the environment in the vicinity of a molecular cloud unless the remnant has involved in a cavity produced by the stellar wind of the progenitor star. We discuss this further in §4.

The limits on thermal emission used for the preceding analyses represent an average of the faint parts of the remnant. Clearly the limits will be higher in the bright regions of the SNR. In the upper panel of figure 8, the dashed histogram represents the upper limit for thermal emission from the bright northwestern region of the remnant using the spectral extraction region illustrated in figure 2. Treating the emission region as a simple slab through the remnant, the upper limit at the low end of the temperature scale limits the preshock density of material at this position to $n_0 < 1D_6^{-1/2} f^{-1/2} \text{ cm}^{-3}$ where f represents the fraction of the slab volume that is actually responsible for the emission. This limit suggests that the ambient density toward the northwest could be considerably greater

3.2.3. Central Source

The best spectral fit for the unidentified central X-ray source 1WGAJ1713.4–3949 based upon a joint fit to the GIS, SIS, and PSPC is obtained for a blackbody spectrum with $kT = 0.38 \pm 0.04$ keV (see Table 2). The normalization yields a relatively small emitting area with radius $R = 3.0_{-0.7}^{+1.0} D_6$ km, suggesting a compact object. The lack of an optical counterpart supports the interpretation that the source is a neutron star associated with G347.3–0.5. However, the blackbody temperature is rather high for a cooling neutron star. Temperatures sim-

ilar to that observed are often associated with emission from heated polar caps, but in the case of 1WGAJ1713.4–3949 the emitting area A is considerably larger than that observed from other sources (e.g. PSR 1919+10; Yancopoulos, Hamilton, & Helfand 1994), implying that 1WGAJ1713.4–3949 may be a rapidly spinning object ($A \propto P^{-1}$, where P is the rotation period).

There is no evidence of long-term flux variability between the ROSAT and ASCA observations (although uncertainties in the spectral model do not allow us to rule out small variations). We extracted a total of 1100 counts in the GIS data from the region around the source for use in timing analysis. A search for pulsations for periods longer than ~ 30 ms (the highest time resolution for the entire data set) yielded negative results implying a pulsed fraction upper limit of $\sim 55\%$ for the extracted events assuming a sinusoidal light curve (Vaughan et al. 1994). Based upon fits to the background-subtracted spectrum for the source, $\sim 47\%$ of the events in the extraction region were attributable to the source. The derived upper limit to the source pulsed fraction is thus of order 100% and offers no meaningful constraint.

We note that adequate spectral fits for the central source emission can also be obtained for power law and Raymond-Smith models. For the power law model, the spectral index is extremely steep (photon index $\Gamma = 4.7_{-0.4}^{+0.5}$) and the column density is large ($N_H = (1.4 \pm 0.2) \times 10^{22} \text{ cm}^{-2}$). For the thermal plasma model, the best-fit column density is $N_H = (1.8 \pm 0.2) \times 10^{22} \text{ cm}^{-2}$ which is comparable with the total absorption through the Galaxy in this direction. Thus it is possible that the source is extragalactic, although the steep X-ray spectral slope and the lack of radio emission makes this interpretation somewhat implausible.

4. DISCUSSION

Based upon all observations to date, a complete picture of G347.3–0.5 is only just beginning to unfold. Initial X-ray observations (Pfeffermann & Aschenbach 1996) indicated a nearby (~ 1 kpc) remnant which was subsequently suggested as a counterpart to a guest star from AD393 (Wang, Qu, & Chen 1997). The latter authors argue that the limited information available for such a scenario would seem to suggest a Type Ib/Ic progenitor explosion. They further suggest that the morphology of the remnant may show some evidence of a central ring-like structure which could be associated with evolution in a wind-blown bubble. We see no evidence of such structure in either the original PSPC maps of G347.3–0.5 nor in our maps obtained with ASCA. Further, as argued above, a distance as small as 1 kpc appears to be very unlikely.

The ASCA spectra for G347.3–0.5 clearly indicate the presence of very high energy electrons, providing evidence for direct acceleration of particles by the SNR shock. Reynolds (1998) provides a thorough discussion of the maximum energy constraints for diffusive shock acceleration in SNRs and produces model results for the nonthermal radiation assuming a constant magnetic field and explosion characteristics typical of Type Ia progenitors. The maximum energy for the accelerated particles is determined by: (1) radiative losses by the particles in the ambient magnetic/photon field; (2) the finite acceleration time associated with the SNR age; and (3) particle escape due to the weakening or absence of magnetohydrodynamic waves (beyond some maximum wavelength) from which the electrons scatter. Reynolds (1998) shows that all young SNRs should

show some evidence of nonthermal X-rays due to shock acceleration, but that the maximum ratio of X-ray/radio nonthermal emission will occur when the SNR age is roughly equal to the loss time for electrons in the postshock magnetic field – a condition that apparently holds for SN 1006 but not for other historical SNRs. The nonthermal emission persists to ages beyond 10^4 yr.

A similar scenario for the nonthermal emission in G347.3–0.5 presents some difficulties. We have argued that the distance to this SNR is of order 6 kpc and that it appears to be in the vicinity of a molecular cloud complex. The conditions are thus considerably different than the high-latitude, Type Ia environment for SN 1006. However, if G347.3–0.5 were the result of an explosion in a stellar wind bubble, there are at least qualitative similarities. The surrounding medium would have low density and a toroidal magnetic field which may yield conditions for efficient particle acceleration. Tenorio-Tagle et al. (1991) have performed 2D numerical hydrodynamical simulations of young Type II SNRs interacting with wind-blown bubbles and find that the freely moving ejecta undergo only partial thermalization while the remnant as a whole ages rapidly since early evolutionary phases are essentially accelerated due to the low density medium in the interior of the bubble. If, upon encountering the bubble wall, diffusive shock acceleration is enhanced, the under-thermalization of the ejecta along with the small swept-up mass may result in a large ratio of non-thermal/thermal X-ray emission. Thus, if the remnant is indeed interacting with the observed molecular clouds, this could enhance the nonthermal component. Simulations indicate that such interactions result in additional shocks in the cloud which can enhance the nonthermal electron population (Jun & Jones 1999) although Jones & Kang (1993) argue that such enhancements occur primarily when the incident shock is already dominated by cosmic-ray pressure.

An alternative interpretation for the featureless X-ray spectrum from G347.3–0.5 could be thermal emission from material dominated by low-Z elements (H, He, C, O) which are fully ionized (Hamilton, Sarazin, Szymkowiak, & Vartanian 1985). Hamilton, Sarazin, & Szymkowiak (1986) proposed a scenario for SN 1006 in which the ejecta from the Type Ia explosion were stratified in such a way as to yield an outer region dominated by such featureless emission. In addition they were able to obtain an approximately power-law spectral form by integrating over the power-law distribution of thermal components that came out of their dynamical model. However, Koyama et al. (1995) argue convincingly that their ASCA observations of SN 1006 rule this model out. A similar scenario has been revisited by Laming (1998) who concludes that the flux associated with the featureless components of SN 1006 and G347.3–0.5, if interpreted as thermal in nature, would imply an X-ray emitting mass of low-Z elements far in excess of that expected to be ejected by a Type Ia supernova explosion. Thus, while this mechanism could potentially explain some small featureless components (e.g. for IC443 or Cas A) it does not appear to be a viable explanation for the spectrum of G347.3–0.5. Recent model calculations by Baring et al. (1999) suggest that the soft X-ray flux of young remnants with parameters typical of Type Ia explosions should be dominated by bremsstrahlung emission. However, these authors do find models that produce spectra dominated by synchrotron emission up to and beyond 10 keV. One of these (their model “D”) uses $E_{51} = 10$, ambient density $n_0 = 10^{-3} \text{ cm}^{-3}$, ejecta mass $M_{ej} = 10M_\odot$, and an age of 40,000 yrs. With the exception of the explosion energy (which

is probably unrealistically large anyway), these parameters are moderately consistent with a picture in which G347.3–0.5 is a moderate age SNR which is in a low density environment.

The characteristics of the unidentified X-ray source 1WG AJ1713.4–3949 are marginally consistent with those for a neutron star. The high X-ray to optical flux ratio virtually rules out a stellar counterpart but is consistent with the source being a neutron star. The lack of detected pulsations at current sensitivities does not provide a strong discriminator in the interpretation. The spectral characteristics of the blackbody model provide a curious scenario if accurate, however. The luminosity implied by the spectral fit is considerably higher than expected for hot polar cap models unless the neutron star is spinning with a period of $\lesssim 6$ ms. With the rather sparse spectrum, it is conceivable that an additional spectral component (e.g., softer blackbody emission from the entire surface) is contributing to the somewhat high flux. Alternatively, as mentioned earlier, the source could be an extragalactic background object unrelated to the SNR. More sensitive X-ray measurements are needed to address this.

If 1WG AJ1713.4–3949 is indeed a neutron star associated with G347.3–0.5, then G347.3–0.5 differs from SN 1006 in a very fundamental way in that the latter is the remnant of a Type Ia explosion. Association with the molecular cloud seen in CO would lead to a similar conclusion; the remnant presumably then originated from a high mass progenitor which, in its short lifetime, did not migrate far from its birthplace. Models for cosmic ray production from shell-type remnants would thus need to accommodate the very different environments expected from the two types of progenitors. In this case, we expect the evolution of G347.3–0.5 to have initially been dominated by the effects of a precursor wind cavity. If our preferred distance of 6 kpc, as suggested by the apparent association with the molecular cloud complex, is correct, then the remnant now has a radius of over 50 pc which is still well within the expected size of the stellar wind bubble for massive O-type stars (Chevalier & Liang 1989). This could provide a logical explanation for both the low density inferred from the lack of thermal X-ray emission as well as the presence of a molecular cloud interaction site.

5. CONCLUSIONS

The strong nonthermal X-ray emission observed from G347.3–0.5 provides tantalizing evidence for the second case of a direct signature of cosmic ray acceleration in SNRs. Like SN 1006, this remnant is very faint in the radio. The peak radio surface brightness of SN 1006 is $\sim 90 \text{ mJy beam}^{-1}$ at the same frequency and resolution, which is comparable to Arc 2 of G347.3–0.5. However, in distinct contrast, G347.3–0.5 shows no evidence of the thermal X-ray emission typically associated with ISM and ejecta material heated by the SNR shock, nor is the morphology as distinctly shell-like as SN 1006.

We have shown that nonthermal X-ray emission pervades the entire image of G347.3–0.5. Faint radio emission appears to delineate a nearly complete shell with brighter arc-like features along regions of bright X-ray emission. CO observations suggest that these features coincide with a region in which the SNR may be interacting with a molecular cloud found along the line of sight. Several lines of evidence, including an association with this molecular cloud complex as well as an H II region, suggest that the most appropriate distance to the remnant is 6 kpc. The lack of thermal emission sets a strong limit on the mean density around the remnant: $n_0 < 0.28D_6^{-1/2} \text{ cm}^{-3}$. Al-

though this is rather low for the near vicinity of a molecular cloud, we argue that it means the majority of the remnant is evolving in the low density interior of the large circumstellar cavity driven by the wind of its massive progenitor star. Simple Sedov-phase models for the remnant's evolutionary state can be found that are consistent with this low density environment for reasonable values of the age and explosion energy. However in the absence of an actual measurement of the thermal properties of the remnant, any conclusions about the evolutionary state of the remnant remain premature. In the X-ray bright region toward the northwest edge of G347.3–0.5, where an interaction with denser gas may be occurring, the limits on the ambient density are higher $n_o < 1D_6^{-1/2} \text{ cm}^{-3}$ and broadly consistent with the densities estimated around other SNRs that are associated with molecular clouds (e.g., N132D in the Large Magellanic Cloud, see discussion in Hughes, Hayashi, and Koyama 1998). Regardless of its precise evolutionary state, our observations reveal G347.3–0.5 to be the most extreme example known of a nonthermal shell-type X-ray remnant and may indicate that shock acceleration of cosmic rays by supernova remnants can occur in a diversity of interstellar environments.

Additional measurements will help shed light on the nature of G347.3–0.5. In particular, a search for OH maser emission (Frail et al. 1996) along the NW limb could confirm a molecular cloud interaction there. Optical observations of this region could also provide evidence of such an interaction, but the extinction is rather high making such observations diffi-

cult. Deeper X-ray observations which might reveal and characterize the thermal component are needed, as are additional observations of the centrally-located source in order to assess the potential for association as the compact relic of the explosion which produced G347.3–0.5. While the X-ray spectrum of the SNR clearly indicates the presence of very high energy electrons, and by inference the acceleration of cosmic rays, further study is required to provide a sufficiently constrained picture of G347.3–0.5 to which acceleration models can be compared. Higher-energy X-ray observations to search for any change in the spectral index which might be associated with a bremsstrahlung component will be important in this regard, as will higher-resolution spatial and spectral observations to provide additional information on the shock structure, and more sensitive observations to search for thermal emission.

We gratefully acknowledge T. Handa and T. Hasegawa of the University of Tokyo who kindly shared their CO(2–1) observations in the vicinity of G347.3–0.5 prior to publication. The MOST is operated by the University of Sydney with support from the Australian Research Council and the Science Foundation for Physics within the University of Sydney. BMG acknowledges the support of an Australian Postgraduate Award. This work was supported in part by the National Aeronautics and Space Administration through contract NAS8-39073 and grant NAG5-4803. JPH acknowledges support through NASA grants NAG 5-4794 and NAG 5-4871.

REFERENCES

Allen, G. et al. 1997, *ApJ* 487, L97
 Baring, M. G., Ellison, D. C., Reynolds, S. P., Grenier, I. A., & Goret, P. 1999, *ApJ* – to appear in Vol. 513, March 1
 Bitran, M., Alvarez, H., Bronfman, L., May, J., & Thaddeus, P. 1997, *A&AS* 125, 99
 Bronfman, L., Alvarez, H., Cohen, R. S., & Thaddeus, P. 1989, *ApJS*, 71, 481
 Burton, W. B. 1985, *A&AS* 62, 365
 Burton, W. B. 1988, in *Galactic and extragalactic radio astronomy* (2nd edition). Berlin and New York, Springer-Verlag, 1988, p. 295–358
 Chiar, J. E., Kutner, M. L., Verter, F., & Leous, J. 1994, *ApJ*, 431, 658
 Chevalier, R. A., & Liang, R. P. 1989, *ApJ*, 344, 332
 Condon, J. J., Griffith, M. R., Wright, A. E. 1993, *AJ*, 106, 1093
 Cox, D. P. & Anderson, P. R. 1982, *ApJ*, 253, 268
 Dame, T. M., Elmegreen, B. G., Cohen, R. S., Thaddeus, P. 1986, *ApJ* 305, 892
 Dickey, J. M., & Lockman, F. J. 1990, *ARA&A*, 28, 215
 Frail, D. A., Goss, W. M., Reynolds, E. M., Giacani, E. B., Green, A. J., Otrupcek, R. 1996, *AJ* 111, 1651
 Hamilton, A. J. S., Sarazin, C. L., & Szymkowiak, A. E. 1986, *ApJ* 300, 698
 Hamilton, A. J. S., Sarazin, C. L., Szymkowiak, A. E., & Vartanian, M. H. 1985, *ApJ*, 297, 5
 Hughes, J. P., Hayashi, I., & Koyama, K. 1998, *ApJ*, 505, 732
 Jones, T. W., & Kang, H. 1993, *ApJ*, 402, 560
 Jun, B.-I., & Jones, T. W. 1999 – accepted for publication in *ApJ*
 Kennel, C. F., & Coroniti, F. V. 1984, *ApJ*, 283, 694
 Keohane, J. W., Petre, R., Gotthelf, E. V., Ozaki, M., & Koyama, K. 1997, *ApJ* 484, 350
 Koyama, K., Petre, R., Gotthelf, E. V., Hwang, U., Matsura, M., Ozaki, M., & Holt, S. S. 1995 *Nature* 378, 255
 Koyama, K. et al. 1997, *PASJ* 49, L7
 Laming, M. J. 1998, *ApJ* 499, 309
 Large, M. I., Campbell-Wilson, D., Cram, L. E., Davison, R. G., Robertson, J. G. 1994, *PASA* 11, 44
 Lockman, F. J. 1979, *ApJ* 232, 761
 Pfeffermann, E. & Aschenbach, B. 1996, in *Roentgenstrahlung from the Universe*, MPE Report 263, p267
 Raymond, J. C. & Smith, G. W. 1977, *ApJS* 35, 49
 Reynolds, S. P. 1996, *ApJL* 459, L13
 Reynolds, S. P. 1998, *ApJ*, 493, 375
 Roberts, D. A., Goss, W. M., Kalberla, P. M. W., Herbstmeir, U., & Schwarz, U. J. 1993, *A&A*, 274, 427
 Robertston, J. G., 1994, *Proc Astr Soc Aust*, 11, 44
 Sakamoto, S., Hasegawa, T., Hayashi, M., Handa, T., & Oka, T. 1995, *ApJS*, 100, 125
 Saken, J. M., Fesen, R. A., & Shull, J. M. 1992, *ApJS*, 81, 715
 Sedov, L. 1959, *Similarity and Dimensional Methods in Mechanics* (New York: Academic)
 Seta, M. et al. 1998, *ApJ*, 505, 286
 Slane, P., Bandiera, R., & Torii, K. 1998 – to appear in a special issue of *Memorie della Societa' Astronomica Italiana (Proceedings)*
 Slane, P., Vancura, O., & Hughes, J. P. 1996, *ApJ*, 465, 840
 Spitzer, L., Jr. 1978, *Physical Processes in the Interstellar Medium* (New York: Wiley-Interscience)
 Stocke, J. T. et al. 1991 *ApJS*, 76, 813
 Strong, A. W. & Mattox, J. R. 1996, *A&A*, 308, L21
 Tanimori, T. et al. 1998, *ApJ*, 497, L25
 Tenorio-Tagle, G., Różyczka, M., Franco, J., & Bodenheimer, P. 1991, *MNRAS*, 251, 318
 Vaughan, B. A. et al. 1994 *ApJ*, 435, 362
 Wang, Z.R., Qu, Q.-Y., Chen, Y. 1997, *A&A*, 318, 59
 Yancopoulos, S., Hamilton, T. T., & Helfand, D. J. 1994, *ApJ*, 429, 832.

This figure "f4.jpg" is available in "jpg" format from:

<http://arxiv.org/ps/astro-ph/9906364v1>

This figure "f5.jpg" is available in "jpg" format from:

<http://arxiv.org/ps/astro-ph/9906364v1>

This figure "f6.jpg" is available in "jpg" format from:

<http://arxiv.org/ps/astro-ph/9906364v1>